Frontiers of Information Technology & Electronic Engineering
www.jzus.zju.edu.cn; engineering.cae.cn; www.springerlink.com
ISSN 2095-9184 (print); ISSN 2095-9230 (online)
E-mail: jzus@zju.edu.cn

# Broadband and asymmetrical Doherty based on circuit parameter solution space*

Cheng BI[1], Haotian LI[2], Shuai WANG[2], Zhijiang DAI[†‡1], Jingzhou PANG[1], Ruibin GAO[1], Kang ZHONG[1], Jingsong WANG[1]

[1]*School of Microelectronics and Communication Engineering, Chongqing University, Chongqing, China*

[2]*The 54th Research Institute of China Electronics Technology Group, Shijiazhuang, Hebei, China*

[†]E-mail: daizj_ok@126.com

Received Mar. 23, 2024; Revision accepted May 30, 2024; Crosschecked

unedited

**Abstract:** In the present paper, the input impedance of the post–matching network (PMN) is configured as a complex value. The parameter solution space is determined based on the fundamental principles of the Doherty power amplifier (DPA), enabling the DPA to achieve high efficiency at the output power back–off(OBO). In this paper, the parameter solution space comprises three variables: the phase parameter of the output matching network for the carrier power amplifier (carrier PA), the phase parameter of the output matching network for the peaking power amplifier (peaking PA), and the input impedance of PMN. These parameters are optimized so as to enable the DPA to achieve high efficiency at the OBO .In this paper, an one–to–one mapping relationship is established between the frequency and the parameter solution space, allowing for a precise optimization of the DPA across a broad frequency range. Leveraging this mapping relation, an asymmetric DPA designed to operate over the 1.8–2.6GHz frequency band is designed and fabricated, demonstrating the feasibility and effectiveness of the proposed approach.Under continuous wave excitation, the test results show that the drain efficiency(DE) is 42.7%–56.4% at 9.5dB OBO and the saturated DE is 45.8%–71.1%. The saturated output power of this DPA is 46.9–48.8 dBm with a gain of 5.5–8.0dB at saturation. Besides, a 20–MHz long–term–evolution (LTE) modulated signal with a peak–to–average power ratio(PAPR) of 8 dB is also applied to the fabricated DPA at 1.8GHz, 2.1GHz and 2.6GHz. Under these conditions and at 8dB OBO, the DPA shows an adjacent channel power ratio(ACPR) always lower than 48 dBc after digital predistortion linearization.

**Key words:** Doherty power amplifier; Output matching network; Parameter solution space
https://doi.org/10.1631/FITEE.2400226 **CLC number:**

## 1 Introduction

Power amplifier(PA) is one of the key components of the mobile communication system and the radar system. It plays a pivotal role in the functioning of the whole system(Li et al., 2022). Stepping into the 5G era, the architecture of large–scale multi–input multiple–output (MIMO) transmitters is the focus of the current research. Therefore, with the increase of the number of frequency bands to be covered by the transmitter, it is imperative to broaden the bandwidth of the RF amplifier(Cavarroc et al., 2023). On the other hand, in order to improve the spectrum efficiency, the modulated signal with high peak–to–average power ratio (PAPR) is usually used, which requires the amplifier to provide efficient performance not only at saturation, but also at the output power back–off (OBO)(Xu et al., 2021). Therefore, the PA that can achieve high efficiency at the OBO is an excellent choice for the industry. In the past few decades, many technologies and ar-

‡ Corresponding author
* Project supported by the National Natural Science Foundation of China (Nos. 62001061, 62371077, and 62171065)
© Zhejiang University Press 2024

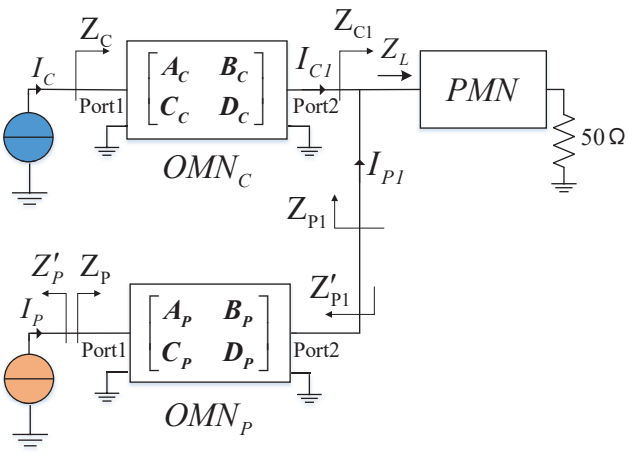


**Figure 1 Topology of the simplified traditional DPA. DPA, Doherty power amplifier.**

chitectures have been proposed to achieve the high efficiency at the OBO, such as Doherty power amplifiers (DPAs)(Doherty, 1936), LMBA(Chen et al., 2023) and outphasing(Li et al., 2021). Among them, the DPA has become one of the most popular technologies because of its simple circuit structure and high reliability. The traditional DPA that uses the same type of transistors in the main circuit and auxiliary circuit can achieve high efficiency at the 6dB OBO, but the broadband performance of the traditional DPA is not very good(Zhang et al., 2023a). Therefore, designing DPAs with a certain bandwidth has become a research hotspot. In 2016, William Hallberg treated the output matching network as a black box whose parameters ((the impedance of carrier PA at the current source plane, the combining impedance ) and the input phase delay are solved according to the given transistor characteristics and design requirements. Based on this theory, a symmetric Doherty PA operating at 2.14 GHz was designed(Hallberg et al., 2016). In 2018, Zhenxing Yang designed a broadband PA operating at 1.1–2.4 GHz using the complex combining load (CCL) with noninfinity peaking impedance(Yang et al., 2019). In 2022, Bachi et al. (2022) proposed a new combiner analysis method for the design of DPAs, based on which Class E PAs operating at 1.1–2.4 GHz were designed in a 130nm RF–SOI process. Nowadays, the modulated signals in communication equipment tend to use the modulated signals with high PAPR, which requires the PA to achieve high efficiency at larger OBO level(larger than 9dB). The traditional DPA only has an OBO of only 6dB. Therefore, in recent years, many scholars have improved the Doherty architecture to achieve high efficiency at greater OBO, such as through multi–way(Zhang et al., 2023b), asymmetric Doherty architecture(Li et al., 2023; Rouhani et al., 2020), and CCL(Fang and Cheng, 2014). In the present study, different transistors are used in the main road and the auxiliary road. This asymmetric structure is used to expand the OBO level. Meanwhile, the input impedance of the post–matching network (PMN) is designed as a complex value, and then the solution space $[\theta_C, \theta_P, Z_L]$ that makes the DPA achieve high efficiency at the OBO is solved. The one–to–one mapping relationship is set between the frequency and $[\theta_C, \theta_P, Z_L]$ so that these three parameters vary linearly with frequency. Based on the mapping relationship, an asymmetric DPA working over 1.8–2.6GHz is designed using GaN HEMT devices. The remaining portions of this paper are summarized as follows: In Section II, finding the solution space and setting the relationship between the frequency and the solution space are performed. Section III shows the detailed design procedure of this DPA. The simulation and measurement results are presented in Section IV. The conclusion is given in Section V.

unedited

## 2 Theoretical analysis of the proposed DPA

### 2.1 Expand the OBO level by using asymmetric cells

The simplified schematic of the traditional DPA is shown in Fig.1. The DPA consists of two amplifiers: a class–B biased carrier PA(main) and a class–C biased peaking PA(auxiliary). Two current generators($I_C$ and $I_P$) represent the carrier PA and the peaking PA, respectively. The principle of the DPA is to increase the impedance at the current source plane ($Z_C$ in Fig.1) at the OBO level so that the voltage of the carrier PA can reach saturation, thus improving the efficiency. The OMNc is the output matching network of carrier PA. OMNp is the output matching network of peaking PA. PMN represents the post–matching network. If the carrier PA and the peaking PA use the same drain bias voltage, the OBO level of the DPA can be defined as in Eq. (1), where $\delta$ is the ratio of $I_{C1}$ and $I_{P1}$ in the saturated state(Pang et al., 2016; Son et al.,

2011). $I_{C1}$ and $I_{P1}$ represent the current of carrier PA and peaking PA at the combining point, respectively. According to the traditional DPA theory, $Z_C$, $Z_P$(the impedance of carrier PA and peaking PA at the current source plane, respectively), $Z_{C1}$ ,$Z_{P1}$(the impedance of carrier PA and peaking PA at the combing point, respectively) and $Z_L$(the input impedance of PMN) should satisfy the following relationship(Pang et al., 2016).

$$OBO = 20 \cdot \lg(1+\delta) \tag{1}$$

$$Z_C = \begin{cases} (1+\delta)\mathrm{R}_{opt_c} & \text{OBO} \\ \mathrm{R}_{opt_c} & \text{SAT} \end{cases} \tag{2}$$

$$Z_P = \mathrm{R}_{opt_p} \quad \text{SAT} \tag{3}$$

$$Z_{C1} = \begin{cases} Z_L & \text{OBO} \\ (1+\delta)Z_L & \text{SAT} \end{cases} \tag{4}$$

$$Z_{P1} = \left(1+\tfrac{1}{\delta}\right) Z_L \quad \text{SAT} \tag{5}$$

$$Z_L = \frac{\mathrm{R}_{opt_c}}{\delta+1} \tag{6}$$

In this paper, the carrier PA uses MACOM's CGH40025F transistor with a maximum drain output current of 3A, and the peaking PA uses the CGH40045F transistor of MACOM with a maximum drain output current of 6A. Therefore, $\delta$, the current ratio of the two PAs in the saturated state, is set to 2. The drain biases are both set as 28V. According to Eq. (**??**), the9.5 dB OBO level can be achieved. $R_{opt_c}$ and $R_{opt_p}$ are 18.6$\Omega$ and 9.3$\Omega$, respectively based on $R_{opt} = 2V_{CC}/I_{\max}$(Yang et al., 2019). The impedance $Z_C, Z_P, Z_{C1}, Z_{P1}, Z_L$ can be calculated by Eqs. (**??**)–(6).

## 2.2 Solving the parameter solution space of DPA

The performance of the DPA depends on its efficiency at the OBO. Its efficiency at the OBO is determined by $Z_{CB}$ which is the impedance $Z_C$ at the OBO in Fig.1. The impedance $Z_C$ can be expressed in terms of the ABCD parameters as given by (Li et al., 2019):

$$Z_C = \frac{A_C \cdot Z_{C1} + B_C}{C_C \cdot Z_{C1} + D_C} \tag{7}$$

Therefore, in order to calculate the impedance $Z_{CB}$, four parameters of the ABCD matrix of OMNc and $Z_{C1B}$ which is the impedance $Z_{C1}$ at the OBO are required to be calculated.

### 2.2.1 Solving the ABCD Matrix of PAs

In order to obtain the ABCD matrix of OMNc, the scattering coefficient can be calculated first. According to Fig. 1, set the reference impedance of port 1 of OMNc as $R_{opt_c}$, and set the reference impedance of port 2 as $(1+\delta)Z_L$. When the Doherty works at saturation, port 1 and port 2 of OMNc are connected with the matching impedance. According to the definition of the scattering coefficient, $S_{11} = S_{22} = 0$. Since OMNc is lossless and reciprocal, the scattering coefficient matrix of OMNc is shown in Eq. (8). The scattering coefficient of OMNp can also be analyzed according to the same principle. Set the reference impedance of port 1 of OMNp as $R_{opt_p}$ and set the reference impedance of port 2 of OMNp as $(1+1/\delta\ )Z_L$. The expression of the scattering coefficient matrix is shown in Eq. (9).

$$\begin{bmatrix} S_{11_C} & S_{12_C} \\ S_{21_C} & S_{22_C} \end{bmatrix} = \begin{bmatrix} 0 & e^{j\theta_C} \\ e^{j\theta_C} & 0 \end{bmatrix} \tag{8}$$

$$\begin{bmatrix} S_{11_P} & S_{12_P} \\ S_{21_P} & S_{22_P} \end{bmatrix} = \begin{bmatrix} 0 & e^{j\theta_P} \\ e^{j\theta_P} & 0 \end{bmatrix} \tag{9}$$

According to the above parameters, the ABCD matrix of OMNc and the reference impedance of port 1 and port 2 of OMNc have been obtained. Hence, According to (Frickey, 1994), the ABCD matrix of OMNC can be calculated. The specific expression of OMNc is shown in Eq. (10).

$$\begin{aligned} A_C &= \frac{R_{opt_c}(1+e^{j2\theta_C})}{2e^{j2\theta_C}\sqrt{R_{opt_c}Z_L}} \\ B_C &= \frac{R_{opt_c}(R_{opt_c}\breve{\ }e^{j2\theta_C}Z_L)}{2e^{j2\theta_C}\sqrt{R_{opt_c}Z_L}} \\ C_C &= \frac{1\breve{\ }e^{j2\theta_C}}{2e^{j2\theta_C}\sqrt{R_{opt_c}Z_L}} \\ D_C &= \frac{R_{opt_c}+e^{j2\theta_C}Z_L}{2e^{j2\theta_C}\sqrt{R_{opt_c}Z_L}} \end{aligned} \tag{10}$$

Similarly, the ABCD matrix of OMNp can also be calculated, and the specific expression is listed in Eq.

unedited

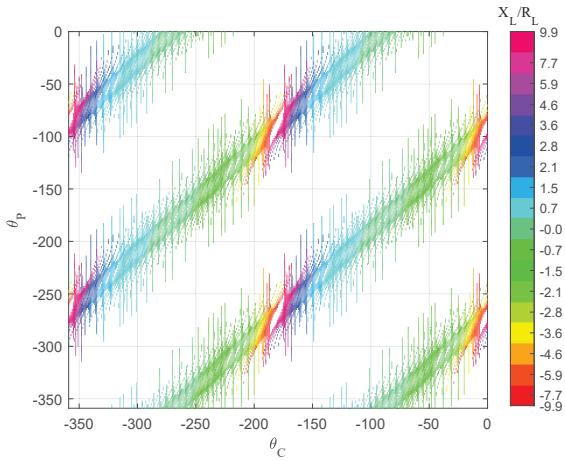


**Figure 2 The parameter solution space $[\theta_C, \theta_P, Z_L]$**

**Table 1 Theoretical parameters at frequencies over 1.8–2.6GHz**

| Frequency (GHz) | $\theta_C$ (°) | $\theta_P$ (°) | $X_L/R_L$ |
|---|---|---|---|
| 1.8 | –45 | –90 | –1 |
| 1.9 | –55 | –100 | –0.69 |
| 2.0 | –59 | –110 | –0.60 |
| 2.1 | –68 | –120 | –0.40 |
| 2.2 | –73 | –130 | –0.31 |
| 2.3 | –79 | –138 | –0.19 |
| 2.4 | –84 | –150 | –0.10 |
| 2.5 | –90 | –160 | 0 |
| 2.6 | –95 | –170 | 0.10 |

$^*R_L = R_{opt_c}/3$

(11).

$$\begin{aligned} A_P &= \frac{R_{opt_p}(1+e^{j2\theta_P})}{2e^{j2\theta_P}\sqrt{R_{opt_p}Z_L}} \\ B_P &= \frac{R_{opt_p}(R_{opt_p}\breve{}e^{j2\theta_P}Z_L)}{2e^{j2\theta_P}\sqrt{R_{opt_p}Z_L}} \\ C_P &= \frac{1\breve{}e^{j2\theta_P}}{2e^{j2\theta_P}\sqrt{R_{opt_p}Z_L}} \\ D_P &= \frac{R_{opt_p}+e^{j2\theta_P}Z_L}{2e^{j2\theta_P}\sqrt{R_{opt_p}Z_L}} \end{aligned} \tag{11}$$

### 2.2.2 Calculate $Z_{C1}$ at OBO

When the DPA works at the OBO, the impedance $Z'_{P1}$ in Fig.1 (the impedance looking into OMNp at the combing point) is not infinite and can be considered as a passive impedance(Shi et al., 2017). Therefore, $Z_{C1B} = Z'_{P1B}||Z_L$, and $Z'_{P1B}$ is $Z'_{P1}$ at the OBO. Subsequently, analyze the specific value of $Z'_{P1B}$. Based on the nature of the reciprocal networks: $AD\breve{}BC = 1$ and Eq. (7), the impedance expression of $Z'_{P1}$ can be derived as shown in Eq.

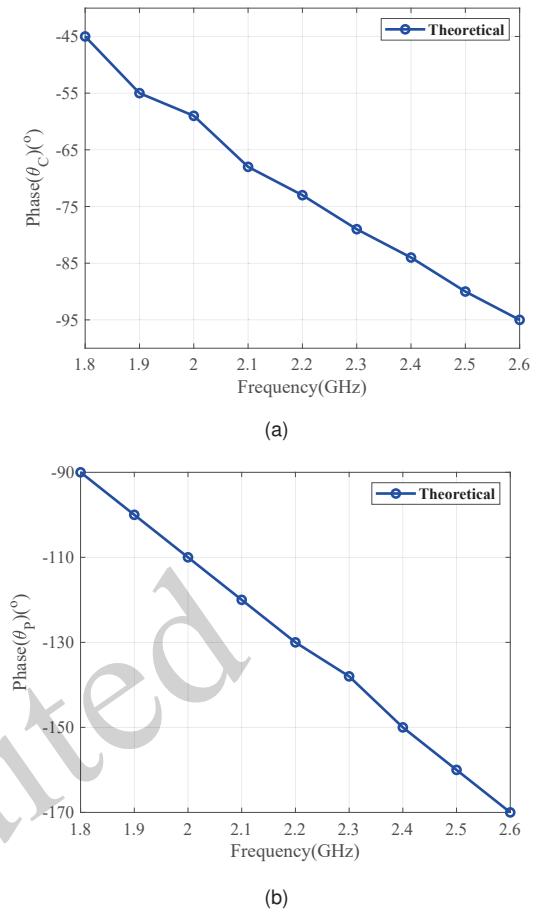


**Figure 3 Theoretical $\theta_C$ of OMNc over the working frequency band (a), Theoretical $\theta_P$ of OMNp over the working frequency band (b)**

(12). When the peaking PA is not turned on, $Z'_P$ can be regarded as infinite and the expression of $Z'_{P1B}$ which is the impedance of $Z'_{P1}$ at the OBO is shown in Eq. (13). The expression of $Z_{C1B}$ is shown in Eq. (14).

$$Z'_{P1} = \frac{D_P \cdot Z'_P + B_P}{C_P \cdot Z'_P + A_P} \tag{12}$$

$$Z'_{P1B} = \frac{D_P}{C_P} \tag{13}$$

$$Z_{C1B} = Z_L||Z'_{P1B} = \frac{Z_L \cdot D_P}{Z_L \cdot C_P + D_P} \tag{14}$$

By substituting Eq. (14) into Eq. (7), the value of $Z_{CB}$ is related to the coefficient of the ABCD matrix of OMNc and OMNp, as shown in Eq. (15). According to Eqs. (10)–(11), It can be derived that $Z_{CB}$ is determined by the phase characteristic $\theta_C$ of OMNc and $\theta_P$ of OMNp.

$$Z_{CB} = \frac{A_C D_P Z_L + B_C(Z_L C_P + D_P)}{C_C D_P Z_L + D_C(Z_L C_P + D_P)} \tag{15}$$

unedited

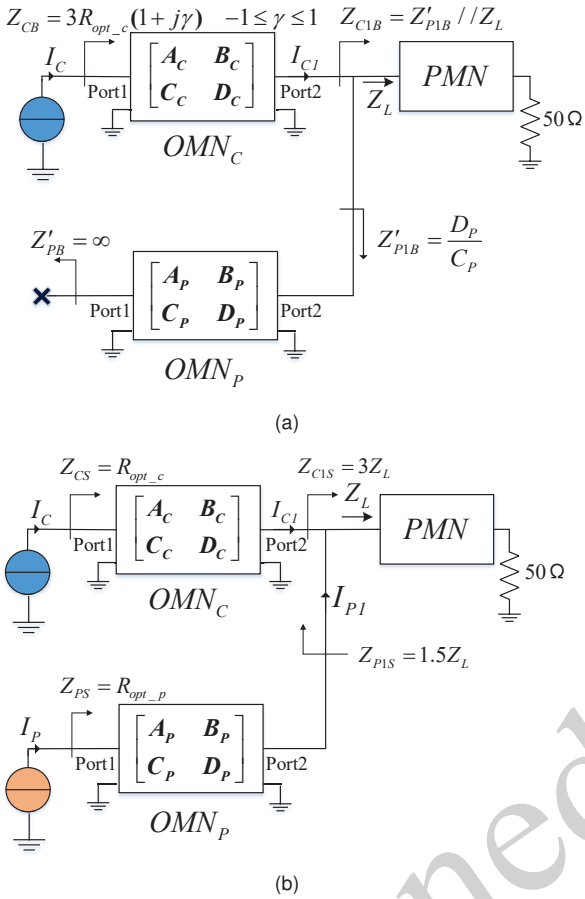


**Figure 4 The output matching network at the OBO (a), The output matching network at saturation (b). OBO, output power back–off.**

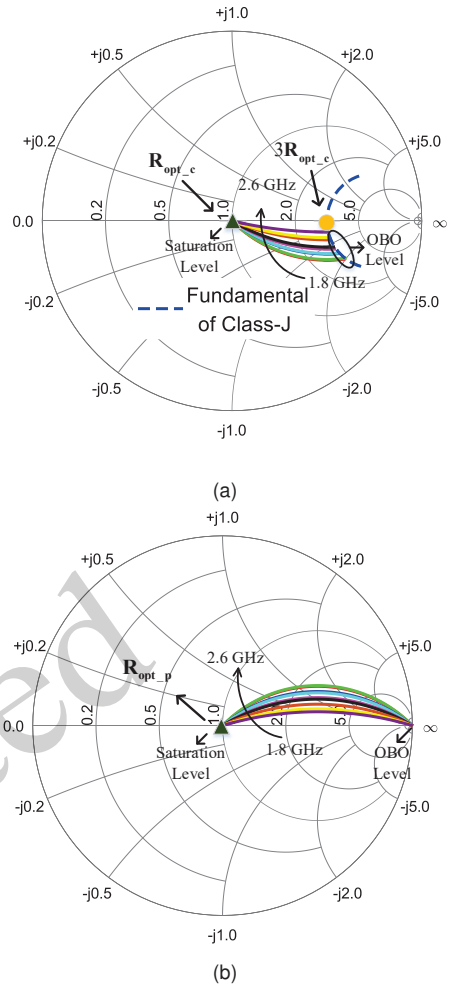


**Figure 5 Theoretical trajectory of $Z_C$ from the OBO to the saturation level across the working frequency band (a), Theoretical trajectory of $Z_P$ from the OBO to the saturation level across the working frequency band (b). OBO, output power back-off.**

unedited

Set $Z_L$ as a complex value: $Z_L = R_L + jX_L$. The real part of $Z_L$ is a fixed value: $R_L = R_{opt_c}/(\delta+1)$. Giving a wide range to the imaginary part $X_L$ of the complex impedance $Z_L$ .Hence, a free parameter $X_L$ will be obtained to extend the high–efficiency range of the designed DPA. Then, set the range of $\theta_C$ and $\theta_P$: $\theta_C \in (\breve{}360, 0)$, $\theta_P \in (\breve{}360, 0)$. It can be concluded that the impedance $Z_{CB}$ has three variables, namely, the phase parameter $\theta_C$ of OMNc, $\theta_P$ of OMNp, and the input impedance $Z_L$ of PMN. Therefore, $Z_{CB}$ is a function determined by these three variables, that is, $Z_{CB} = f(\theta_C, \theta_P, Z_L)$. In order to make the designed DPA achieve high efficiency at the OBO across a wide frequency band, $Z_{CB}$ should meet the continuous class–J mode(Shi et al., 2018). Fig. 5a gives the fundamental parameter space of the continuous class–J mode(the blue point locus). The fundamental impedance space of the continuous class–J mode is represented in Eq. (16)(Wright et al., 2009). According to Section 2.1, $R_{opt_c}$, $R_{opt_p}$ and $\delta$ are all known, and then, substitute them into $f(\theta_C, \theta_P, Z_L)$.

$$Z_{J1} = (1+\delta)\cdot(1+j\cdot\gamma)\cdot R_{opt_c} \quad \breve{}1 \le \gamma \le 1 \tag{16}$$

In order to find the parameter solution that makes $Z_{CB}$ meet the continuous class–J mode in Eq. (16) a screening method is proposed in Eq.(17). If the difference between the real part of the calculated $Z_{CB}$ and $48(3R_{opt_c})$ is less than or equal to 0.8 $(0.05R_{opt_c})$, and the imaginary part is between $[\breve{}3R_{opt_c}, 3R_{opt_c}]$, this set of variables $[\theta_C, \theta_P, Z_L]$ can be regarded as a subset of the high–efficiency

solution space.

$$\left|\mathrm{Re}\left\{f\left(\theta_C,\theta_P,Z_L\right)\breve{}(\delta+1)R_{opt_c}\right\}\right| \le 0.05R_{opt_c}$$
$$\left|\mathrm{Img}\left\{f\left(\theta_C,\theta_P,Z_L\right)\right\}\right| \le (\delta+1)R_{opt_c} \tag{17}$$

2.2.3 Using the solution set space $[\theta_C, \theta_P, Z_L]$ to design the output network of DPA

Through Section 2.2.2, the parameter solution space is the set of many groups of $[\theta_C, \theta_P, Z_L]$. $\theta_C$, $\theta_P$ and $Z_L$ of each group are corresponding one to one. Therefore, as long as one of the variables has been determined, another variable can be found. According to the general method, $\theta_C$ and $\theta_P$ for the center frequency point are $\breve{}90°$ degrees and $\breve{}180°$ degrees, respectively, which serve as the benchmark for selecting other parameter solutions to assign to other frequency points within the bandwidth. However, we avoid this approach because even if a DPA designed using this method achieves good performance, it cannot validate the correctness of the proposed method. It is quite likely that this good performance may be attributed to the traditional DPA theory. Therefore, select parameter solutions that are far from $[\theta_C, \theta_P] = [\breve{}90, \breve{}180]$ to verify the correctness of the theory. Since the absolute value of the phase characteristics of the passive network composed of microstrip lines will generally increase with frequency, $\theta_C$ and $\theta_P$ chosen should also increase with frequency. In addition, the range of variation of the imaginary part of $Z_L$ with frequency should not be too large, so that it is not convenient for the design of the PMN. The corresponding relationship between the selected parameter solutions and frequencies is shown in Table 1, indicating that the absolute values of $\theta_C$ and $\theta_P$ increase as the frequency increases. Next, OMNc and OMNp are designed. Because $\delta = 2$, the matching impedance of Port1 of OMNc is $R_{opt_c}$, and the matching impedance of Port2 is $3Z_L$; the matching impedance of OMNp of Port1 is $R_{opt_p}$ and the matching impedance of port2 is $1.5Z_L$, as shown in Fig. 4b. The scattering coefficient matrices of OMNc and OMNp are shown in Eq. (8)–(**??**). The variation of $\theta_C$, $\theta_P$ and $Z_L$ with frequency should be consistent with that given in Table 1. According to the Section 2.2.2, at saturation, OMNc and OMNp are in the matching state. The impedance $Z_C$ and $Z_P$ are $R_{opt_c}$ and $R_{opt_p}$, respectively. At the OBO , the fundamental impedance of $Z_C$ is in the continuous class–J mode in Fig. 5(a). Therefore, the designed DPA can achieve high efficiency at both saturation and the OBO. The trajectories of $Z_C$ and $Z_P$ from the OBO to saturation across the working frequency band are given in Fig. 5.

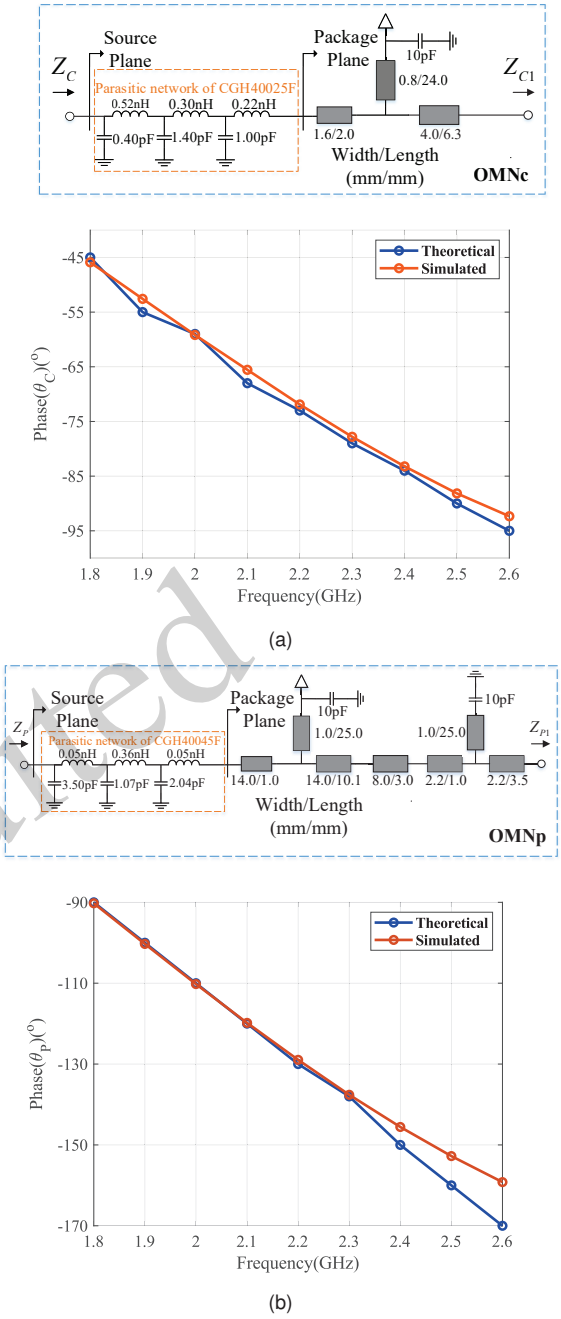


**Figure 6 Schematic and phase parameter of the output matching network (a):OMNc and (b):OMNp**

unedited

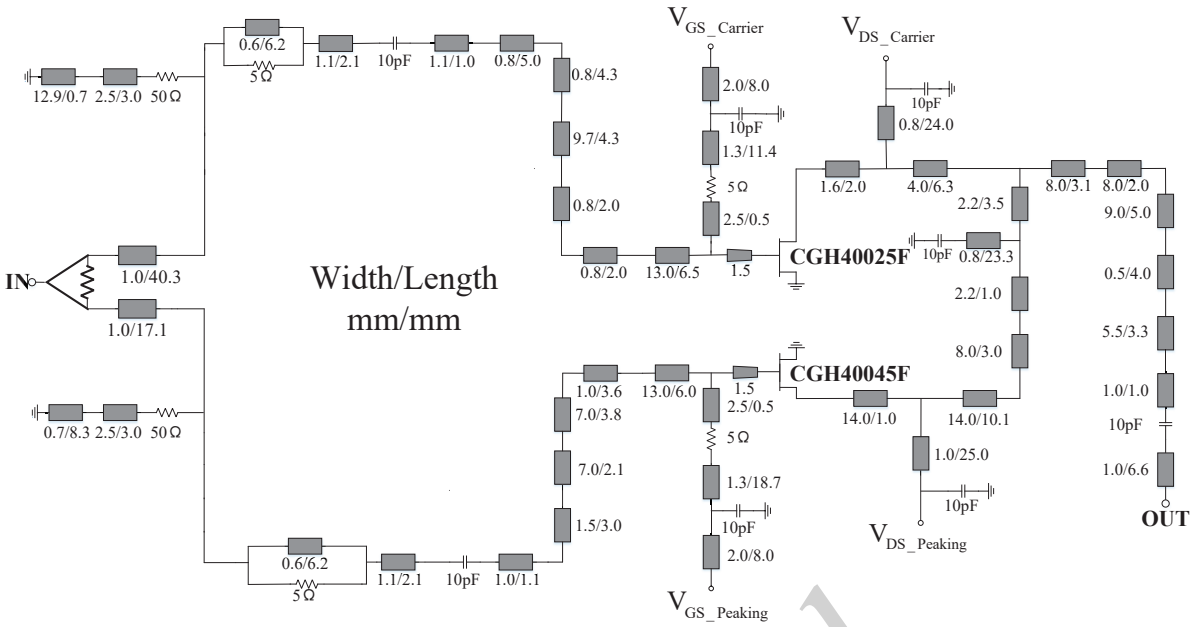


**Figure 9 Schematic of the proposed DPA. DPA, Doherty power amplifier.**

unedited

## 3 Design and simulation

In this section, based on the parameter solution space obtained in Section II, an asymmetric DPA working over 1.8GHz–2.6GHz is designed. The CGH40025F transistor is selected for the carrier PA, whereas the CGH40045F transistor is used for the peaking PA. The maximum current ratio of the peaking PA to the carrier PA is equal to 2. Therefore, the 9.5dB OBO level can be achieved. The circuit is implemented on the substrate of Rogers 4350B with a thickness of H=30 mils and $\varepsilon = 3.48$. The drain bias voltages of the two transistors are both set to 28V. The whole DPA consists of the power divider circuit, input matching network circuit, output matching circuit and PMN. The output matching circuit consists of OMNc and OMNp. Owning to the parasitic effect and packaging elements in the transistor, the packaged elements should be incorporated into OMNc and OMNp. The following goals should be met in the design: (1) when the DPA is in the saturated state, OMNc and OMNp respectively achieve the matching state as shown in Fig.4(b). (2) The phase characteristic of OMNc and OMNp, ($\theta_C$ and $\theta_P$), should be consistent with Table 1. Figs. 6a and 6b show the designed circuit schematic OMNc and OMNp together with the packaged elements. Figs. 6 also shows the curves of $\theta_C$ and $\theta_P$ with frequency, respectively. Among them, the orange line is the phase parameter of Table 1 versus frequency and the blue line is the simulated phase parameter versus frequency. It can be concluded that the simulated results are basically the same as the theoretical results. After completing the design of OMNc and OMNp, a post–matching network(PMN) should be designed to match the 50$\Omega$ antenna load to $Z_L$. PMN is designed based on the relationship between the input impedance $Z_L$ and the frequency given in Table 1. The schematic diagram of the PMN is shown in Fig. 7. The theoretical value of the input impedance is represented by a blue line, and the simulation value is represented by an orange line. Finally, the input matching circuit and the power divider are designed. The function of the input matching circuit is to transmit the signal to the transistor almost lossless. The power divider adopts the three–stage Wilkinson asymmetric power divider and the distribution power ratio of carrier PA and peaking PA is 4:7. The circuit structure of the power divider is shown in Fig. 8. Fig. 9 is the whole circuit diagram. In order to simplify the circuit structure, the circuit structure of the power divider is replaced by its geometry. The actual circuit structure of the power divider is shown in Fig. 8. In order to allow the output current of the carrier PA and the peaking PA maintain the same phase at the combining point at saturation, a phase compensation line is added between the power divider and

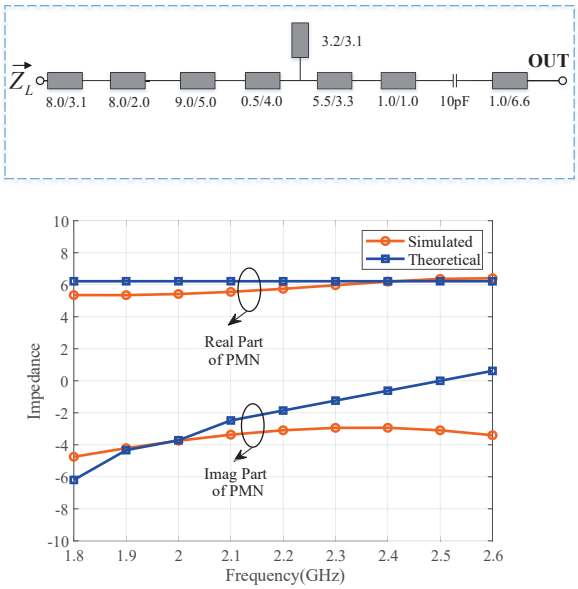


**Figure 7 Schematic of the PMN and its input impedance across the working frequency band. PMN, post–matching network.**

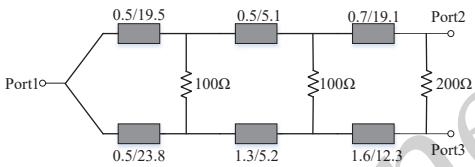


**Figure 8 Schematic of the designed three–stage Wilkinson power divider**

the input matching circuit of the carrier PA. The simulated result of the designed DPA is shown in Fig. 10. The DPA achieves the drain efficiencies of 46.39%–54% and 49.2%–65% at 9.5dB OBO and saturation, respectively. The maximum output power of the designed DPA is 47.2–48.7dBm with a saturation gain of 6–7dB over the whole working frequency band.

## 4 Experimental results

The fabricated DPA is shown in Fig.11. The size of the fabricated DPA is $110mm \times 70mm$. To test the performance of the fabricated DPA, drain efficiency (DE), gain and the adjacent channel power ratio (ACPR) of the designed DPA are tested using the continuous wave and modulated signal, respectively.

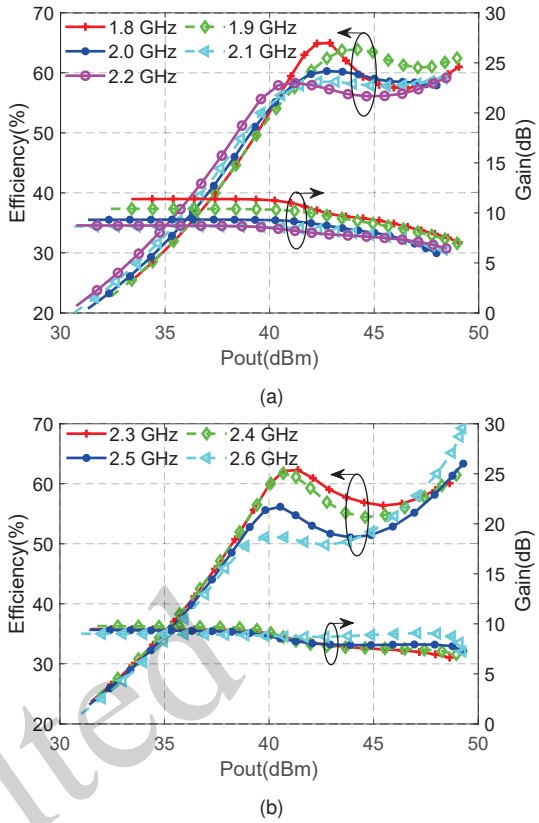


**Figure 10 Simulated drain efficiencies and gains of the designed DPA over output power: (a)1.8–2.2 GHz and (b)2.3–2.6 GHz. DPA, Doherty power amplifier.**

### 4.1 Small–signal measurements

The performance of the fabricated DPA was assessed using a vector network analyzer. Fig. 12 shows the measured S–parameters from 1.8 GHz to 2.6 GHz, alongside simulated data for comparison. For S21, the measured results closely match the simulation, both showing lower gain at higher frequencies. However, there are discrepancies between the measured and the simulated S21 values, likely due to limitations in the accuracy of the simulation model used in ADS.

### 4.2 Continuous–wave measurement

The DE and gain of the fabricated DPA are measured using CW signals across 1.8 GHz–2.6 GHz with the 100 MHz frequency step. Fig. 13 depicts the measurement setup adopted. A vector signal generator (VSG) is responsible for generating the input signal. This signal is then channeled through a driver and an isolator before being fed into the design under the test (DUT). The output signal from

unedited

**Table 2 Performance comparison**

| Reference | Technique | Topology | Frequency (GHz) | FBW (%) | Power (dBm) | OBO (dB) | DE @OBO (%) | DE @SAT (%) | PAE @SAT (%) | ACPR (dBc) |
|---|---|---|---|---|---|---|---|---|---|---|
| (Choi et al., 2021) | Smith chart | Asy. | 1.68 | – | 43.5 | 9.5 | 54.7 | 56.4 | 53.6 | –27.3(1.68GHz) |
| (Li et al., 2022) | Phase compensation | Asy. | 1.55–2.2 | 35 | 45.2–47.3 | 11.1–13.2 | 42.2–52.1 | 47–62.7 | 33.1–51 | –29.1(2 GHz) |
| (Zhou et al., 2022) | Phase compensation | Sym. | 1.6–1.95 | 19.7 | 42.7–43.5 | 9–9.5 | 62.5–67.5 | 64.6–70.9 | 56.5–62.9 | <–22 |
| (Li et al., 2020) | Phase compensation | Sym. | 1.9–2.4 | 23.3 | 44.2–49.7 | 8.5–9 | 44.2–49.7 | 65.2–71.8 | 52.8–56 | –31.1(2.4 GHz) |
| (Xu et al., 2021) | Modified LMN | Asy. | 1.4–2.5 | 56.4 | 44–45.9 | 9 | 44.6–54.6 | 61–75.5 | 53.2–66 | –29.8(1.6 GHz) |
| This Work | Parameter solution space | Asy. | 1.8–2.6 | 36.4 | 46.9–48.8 | 9.5 | 42.7–56.4 | 45.8–71.1 | 36.6–49.7 | –33.6(2.5 GHz) |

ACPR, adjacent channel power ratio; DE, drain efficiency; DPA, Doherty power amplifier; FBW, fractional bandwidth; LMN, load modulation network; OBO, output power back–off; PAE, power added efficiency; Power, saturation output power.

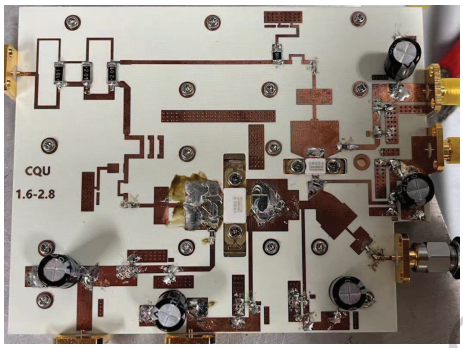


**Figure 11 Photograph of the fabricated DPA. DPA, Doherty power amplifier.**

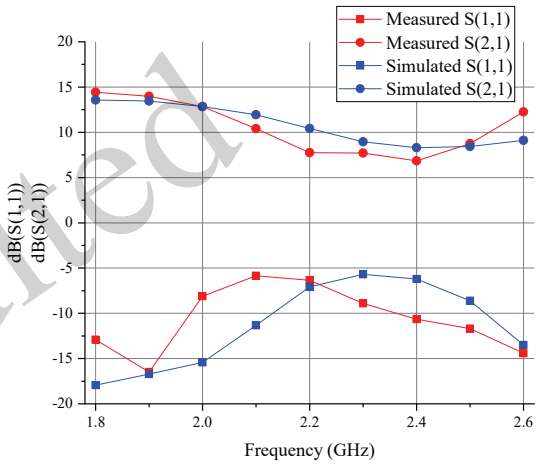


**Figure 12 Simulated and tested S parameter of DPA. DPA, Doherty power amplifier.**

the DPA passes through an attenuator, and ultimately, the measurement results are visualized on a vector spectrum analyzer. When the signal is operated in the frequency range of 1.8–2.0 GHz, the gate bias of the peaking PA is set to –7.5V. When the signal is operating in the frequency range of 2.1–2.6GHz, the gate bias of the peaking PA is set to –8.1V. The drain voltage of both amplifiers are set to 28V. The measured DE and gain are shown in Fig. 14. According to Fig. 14, the DPA can achieve the saturated DE of 45.8%–71.1% with an output power of 46.9dB–48.8dB. At the 9.5dB OBO level, 42.7%–56.4% DE is achieved. The gain at the saturation power is 8.0–5.5dB.In addition,the power added efficiency (PAE) of this fabricated DPA is shown in Fig.15. The DPA can achieve saturated PAE of 36.6%–49.7%. At the 9.5dB OBO level, 26.5%–50.4% PAE is achieved. At high frequencies, the lower gain of the DPA may be caused by mismatch issues between the power divider and the input matching circuit. By comparing Figs. 10 and 14, it can be found that at low frequencies, there is a certain difference between the simulation efficiency curve and the measured efficiency. Analyzing the reason, it may be that there is a certain error between the transistor model used by the ADS simulation platform and the actual transistor. Moreover, the nonlinear capacitance of the transistor has a certain effect on the phase in the actual measurement, which results in the current phase difference at the combining point not being 0, which causes the mismatch of the output matching network and affects the efficiency. In addition, the temperature has an effect on the measured results.

### 4.3 Long–term evolution(LTE) modulated–signal measurements

The high linearity PA can enhance the quality of communications services. Nonlinear distortion

unedited

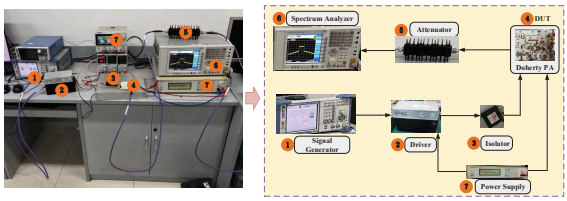


**Figure 13 Large–signal CW signal measurements' setup.**

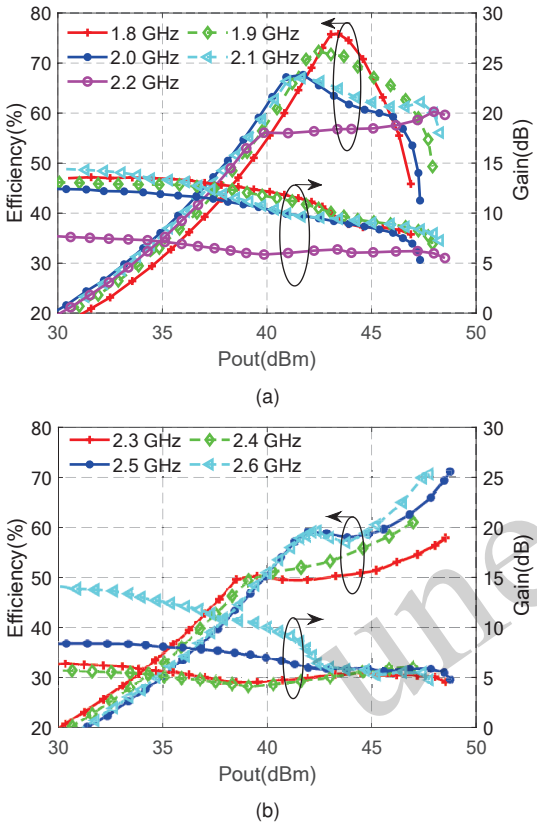


**Figure 14 Measured drain efficiencies and gains of the designed DPA over output power:(a)1.8–2.2 GHz; (b)2.3–2.6 GHz. DPA, Doherty power amplifier.**

will lead to system error, out–of–band radiation and interference with other channels, which seriously affect the quality and reliability of the communication system(Cui et al., 2023). In order to evaluate the linearity of the fabricated DPA, the modulated of 20 MHZ long–term evolution(LTE) signal with a PAPR of 8dB is used. Fig. 16 shows the measured DE, average output power, and the adjacent channel power ratio (ACPR) across the entire band 1.8–2.6 GHz. The DPA achieves an average DE of 42.1%–55.5% and an ACPR of between 23.8dBc and 35.5 dBc in the operation band. An average output power of 38–39.4 dBm is also observed. The normal-

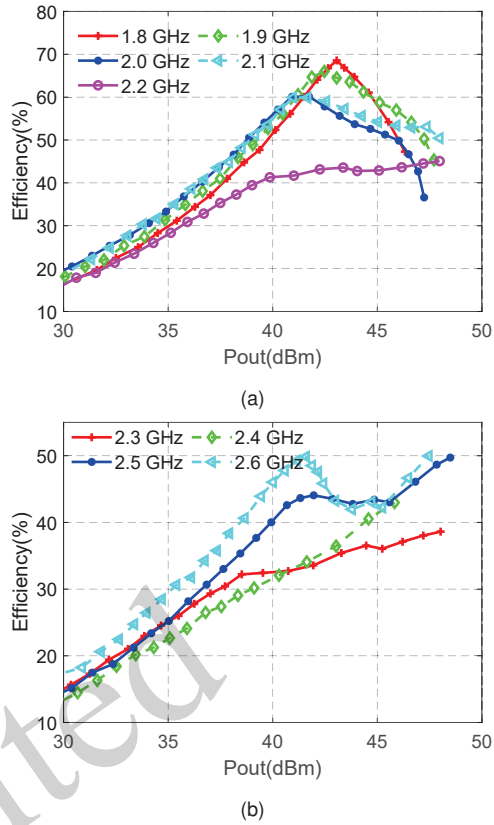


**Figure 15 Measured power–added efficiencies of the designed DPA over output power:(a)1.8GHz–2.2GHz; (b)2.3GHz–2.6GHz.DPA, Doherty power amplifier.**

ized power spectra of the fabricated DPA at 1.8GHz, 2.1 GHz and 2.6 GHz with and without DPDs are displayed in Figs. 18a–c , all of which have been gridded. The output power is 38.1, 36.8dBm and 39dBm with a DE of 54.3%, 55.5% and 51.6%, respectively. Fig. 17 shows the setup for DPD performance measurement. As shown in Fig. 18, better than 49 dBc ACPR is obtained after DPD, more than 20 dB improvement is achieved compared to the original ACPR of PA output signals.The error vector magnitude (EVM) of –10.2dB, –12 dB and –11.4dB is achieved at 1.8 GHz, 2.1 GHz and 2.6 GHz, respectively. After the DPD performed, the EVM can be improved to –37.7dB, –37.1dB and –42dB, respectively, at these three frequencies. The DPD algorithm used is a GMP model under a direct learning structure (closed loop) with ten iterations for the coefficient solution. It has the nonlinearity order Ka =[0:11], memory depth La = [0:4],the nonlinearity of the lagged cross–term order Kb = [0:7], memory depth of the lagged cross–term Lb = [0:4], lagged cross–depth Mb=[0:2], model coefficients of

unedited

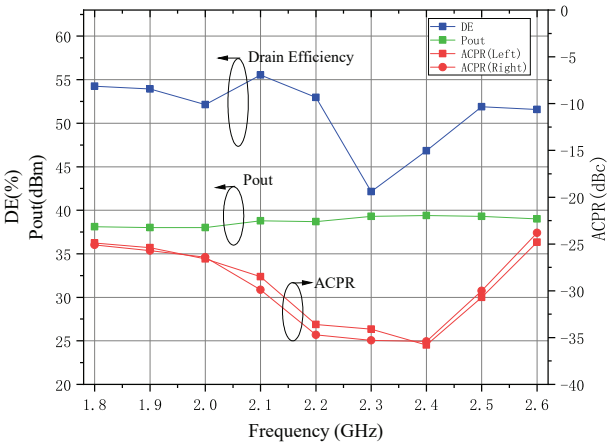


**Figure 16 Measured average DE, average output power and ACLR versus frequency. DE, drain efficiency.**

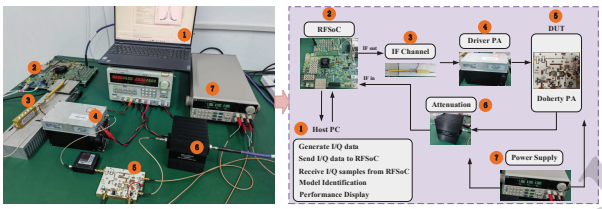


**Figure 17 Setup for DPD performance measurement.**

the leading cross terms Kc=[0:5], and memory depth of leading cross terms Lc=[0:3]. Measured performance is compared to previously reported DPAs with an extended back–off range as given in Table 2. Compared with most of the works in Table 2, the DPA indicated made in this paper shows better broadband performance and efficiency index, with a relative bandwidth of 36%. Besides, this kind of DPA design incorporates transistors with higher saturation power, enabling a significantly higher output power. Additionally, due to the larger size of the transistors utilized in this design, their parasitic parameters are increased and the optimal impedance showed a stronger degree of discreteness, posing considerable challenges in the design process. The DPA designed using the parameter solution space method proposed in this paper has yielded relatively impressive results. This achievement not only validates the correctness of the proposed parameter solution space but also demonstrates its effectiveness in practical design.

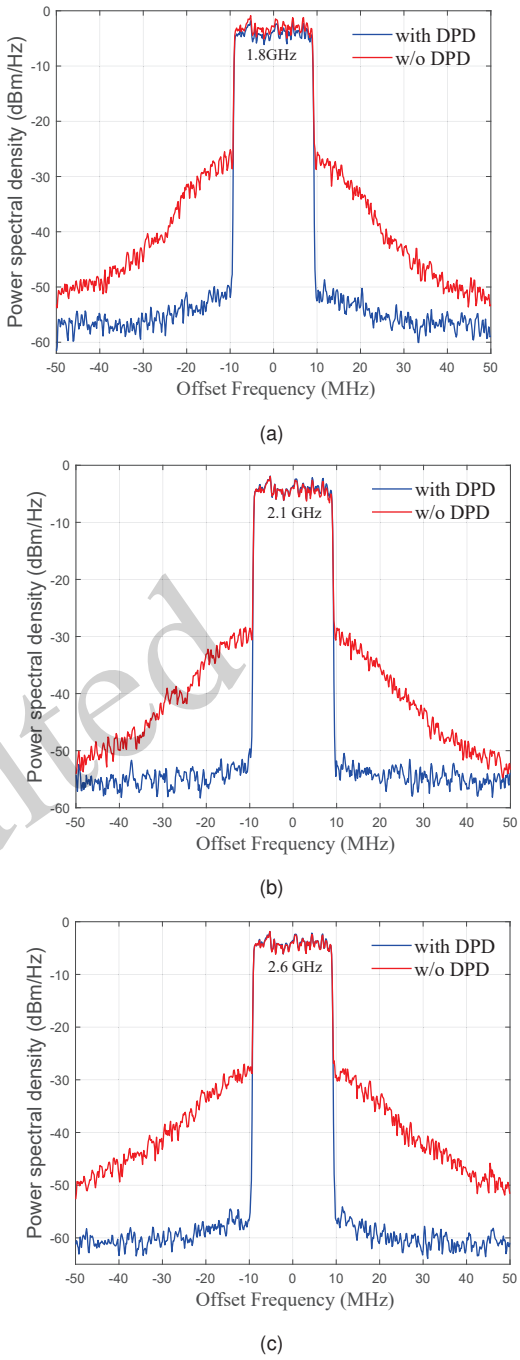


**Figure 18 Measured normalized power spectral density using 20–MHz LTE signals with PAPR=8dB: (a)1.8GHz; (b)2.1GHz and (c)2.6GHz. LTE, long–term evolution; PAPR, peak–to–average power ratio.**

## 5 Conclusions

In this paper, the input impedance of PMN is set to a complex number and the solution set $[\theta_C, \theta_P, Z_L]$ that makes the DPA achieve high effi-

unedited

ciency at the OBO is obtained according to the basic principle of the DPA. Based on this solution set, an asymmetric DPA working over 1.8GHz–2.6GHz is constructed. The DPA can achieve an efficiency of 42.7%–56.4% and 45.8%–71.1% at the 9.5dB OBO level and saturation level. The saturation output power is 46.9dB–48.8dB with a saturated gain of 5.5dB–8.0dB.

## Contributors

Cheng BI, Zhijiang DAI, and Jingzhou PANG designed the research. Cheng BI drafted the paper. Haotian LI, Shuai WANG, Kang ZHONG, Jingsong WANG, and Ruibin GAO helped organize the paper. Zhijiang DAI revised and finalized the paper.

## Conflict of interest

All the authors declare that they have no conflict of interest.

## Data availability

The data that support the findings of this study are available from the corresponding author upon reasonable request.

unedited

## References

Bachi J, Serhan A, Pham DKG, et al., 2022. A novel approach for doherty pa design using a compact l-c combiner. *IEEE Trans Circuits Syst II Express Briefs*, 69(10):4023-4027.
https://doi.org/10.1109/TCSII.2022.3185174

Cavarroc M, Lamy A, Lembeye O, et al., 2023. Compact 40% fractional bandwidth doherty pa with input group delay engineering. *IEEE Microw Wirel Technol Lett*, 33(6):851-854.
https://doi.org/10.1109/LMWT.2023.3266095

Chen WJ, Wu YL, Li SB, et al., 2023. Fully-integrated broadband gaas mmic load modulated balanced amplifier for sub-6 ghz applications. *IEEE Trans Circuits Syst II Express Briefs*, 70(8):2834-2838.
https://doi.org/10.1109/TCSII.2023.3246042

Choi W, Kang H, Oh H, et al., 2021. Doherty power amplifier based on asymmetric cells with complex combining load. *IEEE Trans Microw Theory Tech*, 69(4):2336-2344.
https://doi.org/10.1109/TMTT.2021.3059666

Cui J, Li PP, Sheng WX, 2023. High linearity u-band power amplifier design: a novel intermodulation point analysis method. *Front Inform Technol Electron Eng*, 24(1):176-186.
https://doi.org/10.1631/FITEE.2200082

Doherty WH, 1936. A new high efficiency power amplifier for modulated waves. *Proc Inst Radio Eng*, 24(9):1163-1182.
https://doi.org/10.1109/JRPROC.1936.228468

Fang XH, Cheng KKM, 2014. Extension of high-efficiency range of doherty amplifier by using complex combining load. *IEEE Trans Microw Theory Tech*, 62(9):2038-2047.
https://doi.org/10.1109/TMTT.2014.2333713

Frickey DA, 1994. Conversions between s, z, y, h, abcd, and t parameters which are valid for complex source and load impedances. *IEEE Trans Microw Theory Tech*, 42(2):205-211.
https://doi.org/10.1109/22.275248

Hallberg W, Özen M, Gustafsson D, et al., 2016. A doherty power amplifier design method for improved efficiency and linearity. *IEEE Trans Microw Theory Tech*, 64(12):4491-4504.
https://doi.org/10.1109/TMTT.2016.2617882

Li C, You F, Peng J, et al., 2020. Co-design of matching sub-networks to realize broadband symmetrical doherty with configurable back-off region. *IEEE Trans Circuits Syst II Express Briefs*, 67(10):1730-1734.
https://doi.org/10.1109/TCSII.2019.2946395

Li M, Pang JZ, Li Y, et al., 2019. Ultra-wideband dual-mode doherty power amplifier using reciprocal gate bias for 5g applications. *IEEE Trans Microw Theory Tech*, 67(10):4246-4259.
https://doi.org/10.1109/TMTT.2019.2932977

Li M, Li ZQ, Zheng Q, et al., 2022. A 17–26.5 ghz 42.5 dbm broadband and highly efficient gallium nitride power amplifier design. *Front Inform Technol Electron Eng*, 23(2):346-350.
https://doi.org/10.1631/FITEE.2000513

Li MY, Cheng XB, Dai ZJ, et al., 2023. A novel method for extending the output power back-off range of an asymmetrical doherty power amplifier. *Front Inform Technol Electron Eng*, 24(3):470-479.
https://doi.org/10.1631/FITEE.2200250

Li SS, Huang MY, Jung D, et al., 2021. A mm-wave current-mode inverse outphasing transmitter front-end: A circuit duality of conventional voltage-mode outphasing. *IEEE J Solid-State Circuits*, 56(6):1732-1744.
https://doi.org/10.1109/JSSC.2020.3038882

Pang JZ, He SB, Dai ZJ, et al., 2016. Design of a post-matching asymmetric doherty power amplifier for broadband applications. *IEEE Microw Wirel Compon Lett*, 26(1):52-54.
https://doi.org/10.1109/LMWC.2015.2505651

Rouhani S, Ghanaatian A, Abrishamifar A, et al., 2020. A wideband quasi-asymmetric doherty power amplifier with a two-section matching-phase difference compensator network design using gaas technology. *Analog Integr Circuits Signal Process*, 105(3):359-370.
https://doi.org/10.1007/s10470-020-01731-9

Shi WM, He SB, You F, et al., 2017. The influence of the output impedances of peaking power amplifier on broadband doherty amplifiers. *IEEE Trans Microw Theory Tech*, 65(8):3002-3013.
https://doi.org/10.1109/TMTT.2017.2673822

Shi WM, He SB, Zhu XY, et al., 2018. Broadband continuous-mode doherty power amplifiers with noninfinity peaking impedance. *IEEE Trans Microw Theory*

*Tech*, 66(2):1034-1046.
https://doi.org/10.1109/TMTT.2017.2749224

Son J, Kim I, Moon J, et al., 2011. A highly efficient asymmetric doherty power amplifier with a new output combining circuit. IEEE Int Conf on Microwaves, Communications, Antennas and Electronic Systems, p.1-4.
https://doi.org/10.1109/COMCAS.2011.6105792

Wright P, Lees J, Benedikt J, et al., 2009. A methodology for realizing high efficiency class-j in a linear and broadband pa. *IEEE Trans Microw Theory Tech*, 57(12):3196-3204.
https://doi.org/10.1109/TMTT.2009.2033295

Xu Y, Pang JZ, Wang XY, et al., 2021. Enhancing bandwidth and back-off range of doherty power amplifier with modified load modulation network. *IEEE Trans Microw Theory Tech*, 69(4):2291-2303.
https://doi.org/10.1109/TMTT.2021.3056402

Yang ZX, Yao Y, Li MY, et al., 2019. Bandwidth extension of doherty power amplifier using complex combining load with noninfinity peaking impedance. *IEEE Trans Microw Theory Tech*, 67(2):765-777.
https://doi.org/10.1109/TMTT.2018.2884415

Zhang JR, Zheng SY, Yang N, 2023a. An efficient broadband symmetrical doherty power amplifier with extended back-off range. *IEEE Trans Circuits Syst II Express Briefs*, 70(4):1316-1320.
https://doi.org/10.1109/TCSII.2022.3227045

Zhang XH, Li SS, Huang DQ, et al., 2023b. A millimeter-wave three-way doherty power amplifier for 5g nr ofdm. *IEEE J Solid-State Circuits*, 58(5):1256-1270.
https://doi.org/10.1109/JSSC.2023.3238766

Zhou XY, Chan WS, Sharma T, et al., 2022. A doherty power amplifier with extended high-efficiency range using three-port harmonic injection network. *IEEE Trans Circuits Syst I Regul Pap*, 69(7):2756-2766.
https://doi.org/10.1109/TCSI.2022.3160382

unedited